

Chapman University

Chapman University Digital Commons

Biology, Chemistry, and Environmental Sciences
Faculty Articles and Research

Science and Technology Faculty Articles and
Research

1-5-2021

Rapid Mapping of Landslides in the Western Ghats (India) Triggered by 2018 Extreme Monsoon Rainfall Using a Deep Learning Approach

Sansar Raj Meena
University of Salzburg

Omid Ghorbanzadeh
University of Salzburg

Cees J. van Westen
University of Twente

Thimmaiah Gudiyangada Nachappa
University of Salzburg

Thomas Blaschke
University of Salzburg

Follow this and additional works at: https://digitalcommons.chapman.edu/sees_articles

 [next page for additional authors](#)

Part of the [Environmental Indicators and Impact Assessment Commons](#), [Environmental Monitoring Commons](#), [Other Earth Sciences Commons](#), [Remote Sensing Commons](#), and the [Sedimentology Commons](#)

Recommended Citation

Meena, S.R., Ghorbanzadeh, O., van Westen, C.J. *et al.* Rapid mapping of landslides in the Western Ghats (India) triggered by 2018 extreme monsoon rainfall using a deep learning approach. *Landslides* (2021). <https://doi.org/10.1007/s10346-020-01602-4>

This Article is brought to you for free and open access by the Science and Technology Faculty Articles and Research at Chapman University Digital Commons. It has been accepted for inclusion in Biology, Chemistry, and Environmental Sciences Faculty Articles and Research by an authorized administrator of Chapman University Digital Commons. For more information, please contact laughtin@chapman.edu.

Rapid Mapping of Landslides in the Western Ghats (India) Triggered by 2018 Extreme Monsoon Rainfall Using a Deep Learning Approach

Comments

This article was originally published in *Landslides* in 2021. <https://doi.org/10.1007/s10346-020-01602-4>

Creative Commons License



This work is licensed under a [Creative Commons Attribution 4.0 License](https://creativecommons.org/licenses/by/4.0/).

Copyright

The authors

Authors

Sansar Raj Meena, Omid Ghorbanzadeh, Cees J. van Westen, Thimmaiah Gudiyangada Nachappa, Thomas Blaschke, Ramesh P. Singh, and Raju Sarkar

Rapid mapping of landslides in the Western Ghats (India) triggered by 2018 extreme monsoon rainfall using a deep learning approach

Abstract Rainfall-induced landslide inventories can be compiled using remote sensing and topographical data, gathered using either traditional or semi-automatic supervised methods. In this study, we used the PlanetScope imagery and deep learning convolution neural networks (CNNs) to map the 2018 rainfall-induced landslides in the Kodagu district of Karnataka state in the Western Ghats of India. We used a fourfold cross-validation (CV) to select the training and testing data to remove any random results of the model. Topographic slope data was used as auxiliary information to increase the performance of the model. The resulting landslide inventory map, created using the slope data with the spectral information, reduces the false positives, which helps to distinguish the landslide areas from other similar features such as barren lands and riverbeds. However, while including the slope data did not increase the true positives, the overall accuracy was higher compared to using only spectral information to train the model. The mean accuracies of correctly classified landslide values were 65.5% when using only optical data, which increased to 78% with the use of slope data. The methodology presented in this research can be applied in other landslide-prone regions, and the results can be used to support hazard mitigation in landslide-prone regions.

Keywords Landslides · Convolutional neural network (CNN) · Deep learning · Western Ghats

Introduction

Landslides are one of the most devastating natural disasters in the mountainous regions around the world. Landslides severely damage infrastructure, cause a loss of life and properties, and impact the daily life of people living in the affected regions (Juang et al. 2019). Landslides are of various types, such as debris slides, rock falls, spreads, debris flow, and lahars (Cruden and Varnes 1996). According to Cruden and Varnes (1996), a landslide is ‘the movement of a mass of rock, debris or earth down a slope’. The occurrence of landslides depends on the local terrain, geology and geomorphology of the area, soil types, tectonics, land use, and land cover. In the seismically active regions, landslides are commonly triggered by earthquakes, slope deformation, rock mass movements, and extreme rainfall events (Guzzetti et al. 1999). The situation is worsened by human activities, as instance the development of road networks with road cuts is a widely acknowledged predisposing factor in hilly areas (Das et al. 2011; Xu et al. 2017).

Several approaches have been developed for mapping landslides (Guzzetti et al. 2012; Lu et al. 2011; Martha et al. 2010; Meena et al. 2019; Pradhan et al. 2006; Prakash et al. 2020). The rapid mapping of landslides after an event is still a challenge for disaster management despite the availability of high-resolution satellite images and the algorithms for landslide detection.

Duro et al. (2012) used remote sensing data and semi-automated feature extraction of machine learning models in both pixel- and object-based environments for landslide extraction. In the last decade, the object-based approach has become more common (Jin et al. 2019; Liu et al. 2019; Shahabi et al. 2019; Tavakkoli Piralilou et al. 2019). The recent advancements in the performance of computing platforms have resulted in the development of several machine learning models, including deep learning methods (DLMs). Of the developed DLMs, the deep convolutional neural networks (DCNNs) have been especially widely used for classification and segmentation of satellite images and object detection (Du et al. 2019; Qayyum et al. 2019).

The use of CNN models has yielded very promising results for object classification from aerial images, but only a few studies have assessed landslide detection using the CNN model (see Table 1). Chen et al. (2018) used D-CNN (deep convolutional neural networks) for automated landslide detection in mountainous regions using multi-temporal remote sensing data. Lei et al. (2019) optimized FCN-PP (fully convolutional network within pyramid pooling) for landslide inventory mapping and compared the results with other models, such as the ELSE (employed edge-based level set evolution), RLSE (region-based level set evolution), CDMRF (change detection-based on Markov random field), and CDFFCM (change detection-based fast fuzzy c-means clustering). Ye et al. (2019) used hyperspectral data for landslide detection using DLWC (deep learning with constraints), SID (spectral information divergence), SAM (spectral angle match), and SVM (support vector machine) (Eskandari et al. 2020). Ghorbanzadeh et al. (2019a) evaluated the performance of different CNN models for landslide detection and compared these with three other ML models, namely, ANN, SVM, and RF, using the elevation factor coupled with remote sensing data. Recent studies used different elevation factors combined with remote sensing data for landslide detection using deep learning approaches (Liu et al. 2020; Prakash et al. 2020; Sameen and Pradhan 2019).

In this study, we used the CNN model to detect landslides caused by the extreme rainfall event of August 2018 in the Kodagu district of Karnataka state in the Western Ghats of peninsular India. The extreme rainfall caused deadly floods and landslides in the region (Martha et al. 2019), severely impacting the lives of the local population. Martha et al. (2019) carried out a rapid mapping of the landslides in the affected area using OBIA with Resourcesat-2 LISS-IV images (5.8 m spatial resolution) and reported a total of 771 landslides within an area of 7.1 million m². In this study, we used remote sensing based on 3-m PlanetScope Dove optical satellite imagery and 12.5-m ALOS PALSAR digital elevation data using the CNN model for landslide detection. We compared the resulting landslide inventory based on the CNN model

Table 1 Overview of some recent published studies on the automated mapping of landslides using deep learning approaches

Study	Main objective	Algorithms used	Topographical feature used	Accuracy evaluation methods
Chen et al. (2018)	An automated approach for landslides detection	DCNN	Slope	CE, DP, QP
Lei et al. (2019)	Optimization of (FCN-PP) for landslide inventory mapping	ELSE, RLSE, CDMRF, CDFFCM, CNN, FCN, U-Net, FCN-PP	N/A	Precision, recall, F1-score, OE, accuracy
Ye et al. (2019)	Landslide detection using hyperspectral remote sensing data and comparison of conventional methods with DLWC	DLWC, SVM, SID, SAM	Slope	Overall accuracy, Kappa coefficient, accuracy
Ghorbanzadeh et al. (2019a)	Comparison of different sample patch sizes for landslide detection using deep learning and machine learning	CNN, SVM, D-CNN, RF, ANN	Plan curvature, slope, slope aspect,	Precision, recall, F1-score, mIOU
Sameen and Pradhan (2019)	Landslide detection using residual networks	ResNet, CNN	Altitude, slope, slope aspect, total curvature	Training accuracy, validation accuracy, F1-score, mIOU
Ghorbanzadeh et al. (2019b)	Landslide detection using UAV-derived VHR imagery and topographical factors	CNN	Slope	PPV, TPR, F1-score, OPR, UPR, mIOU
Prakash et al. (2020)	Comparison of pixel-based, object-based, and deep learning methods for landslide detection	RF, ANN, LR, U-Net + ResNet	Hill shade, slope, slope aspect, terrain roughness, curvature, Valley depth, TWI	Accuracy, F1-score, MCC, POD, POFD
Liu et al. (2020)	Post-earthquake landslide extraction using the U-Net model	U-Net, U-Net + ResNet	DSM, slope, slope aspect	Precision, recall, F1-score, mIOU

UAV unmanned aerial vehicle, CNN convolutional neural network, D-CNN deep convolution neural network, FCN fully convolutional network, FCN-PP fully convolutional network within pyramid pooling, ELSE employed edge-based level set evolution, RLSE region-based level set evolution, SVM support vector machine, LR logistic regression, CDMRF change detection-based on Markov random field, CDFFCM change detection-based fast FCM, RF random forest, ResNet residual networks, DLWC deep learning with constrains, ANN artificial neural networks, SID spectral information divergence, SAM spectral angle match

with the manually delineated polygons. Further, we made efforts to enhance the accuracy of the detected landslide polygons by using different training data within a simple CNN architecture.

Study area

Kodagu, also known as Coorg, is a rural district in the state of Karnataka, India, covering an area of 4102 km². The study area is located on the eastern side of the Western Ghats at an elevation ranging from 45 to 1726 m above sea level (Fig. 1). Kaveri, which is the main river in Karnataka, originates in Talakaveri in Kodagu district. Kodagu is predominantly an agricultural region, producing rice and coffee, and various spices like pepper and cardamom and other agroforestry crops are cultivated within the region. The prevalent plantation crop in Kodagu district is coffee. It is the second-largest coffee production region in India after Chikmagalur district, and it accounts for about one-third of India's coffee production. Kodagu is rich in wildlife and has one national park and three wildlife sanctuaries despite being a small district. During the monsoon season (July–August), precipitation is intense and more or less continuous until the end of November. The average annual rainfall is about 4000 mm in hilly region. Heavy rainfall of about 1200 mm occurred during August 2018 (Fig. 2) and caused severe flooding and landslides in the region. The total rainfall that occurred in August exceeded

the amount of the previous 4 years. The total damage caused by the August 2018 landslides was widespread and severe, and the total landslide area was two to three times larger than the landslide areas of the previous 4 years combined. The landslides occurring in our case study area are mainly debris flows. The study area is predominantly hill ranges covering dense forests, plantations, and cultivated valleys (Ramachandra et al. 2019). The study area is characterized by the highly dissected, undulating, and sloping structural hill ranges. Geologically, the study area comprises garnetiferous sericite schists and garnetiferous amphibolite, peninsular gneisses, and biotic gneisses with quartz (Vinutha 2015).

Data used and methodology

Datasets

Inventory dataset

In this study, a training dataset of polygons of the landslides for the Kodagu district was prepared from a manual delineation of landslides based on high-resolution PlanetScope imagery. The satellite images were taken from the Planet Labs Inc. PlanetScope, which includes more than 130 Dove satellites that provide 3 m spatial resolution multispectral images in four bands

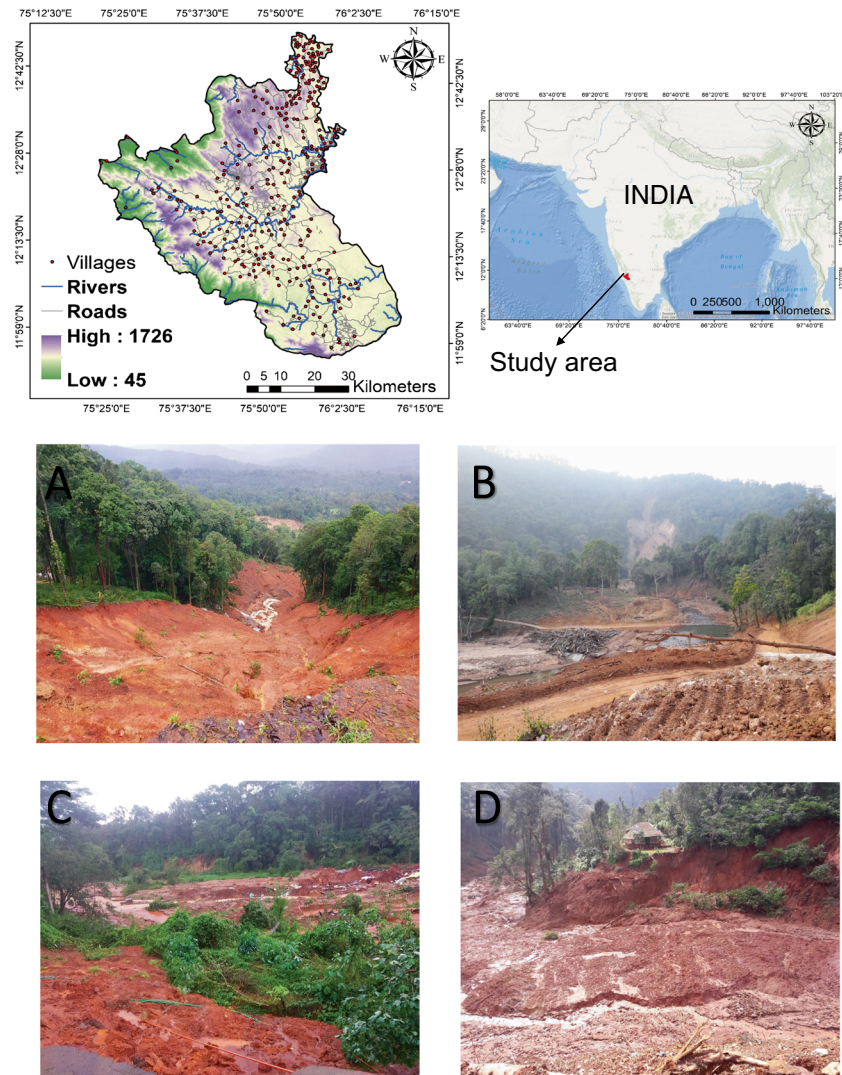


Fig. 1 The location of our study area, with villages, road, and river network. Photographs A–D show landslide features in the area

(RGB, NIR) red, 590–670 nm; green, 500–590 nm; blue, 455–515 nm; and NIR, 780–860 nm (Team 2018). We used cloud-free pre- and post-event PlanetScope images to map the landslide locations manually (Fig. 3). A total of 343 landslides were mapped as polygons, covering an area of 4140 km². The number of detected landslides differs from the 771 landslides reported by another study using object-based image analysis (OBIA) (Martha et al. 2019). This difference likely results from the automated landslide detection algorithm that was used. In our case, the individual parts of the same landslide were often counted as separate polygons, mainly when they were not connected due to the presence of shadows or vegetation in the images. The landslide inventory has different landslide types, namely, mudflows, rock falls, and debris slides. The study area has hilly terrain and the landslide lengths vary, reaching up to 1828 m in length. The smallest manually mapped landslide is 276.23 m² and the largest is 81,342.87 m². Of the total 343 landslides, 93 are mudslides, 23 are rock falls, and 227 are debris-type landslides.

Optical data

In hilly terrain, dissected landscapes with rocks and barren areas show similar spectral characteristics as landslides (Moine et al. 2009). Payne et al. (2019) observed that the red wavelength band provides spectral characteristics of landslides and barren areas in hilly terrain and forest-covered areas. The optical band of single RGB (red, green, blue) is useful for the identification of landslides, but it is not sufficient to differentiate landslides from vegetation growth in a shaded region. In such a case, an additional infrared band is useful to counteract the drawbacks of the mixed spectral response of landslides to only RGB spectral data. For the manual detection of landslides, we used the NDVI layer along with four bands of 3-m spatial resolution PlanetScope Dove imagery. The four PlanetScope spectral bands were used to calculate the normalized difference vegetation index (NDVI), which served as the basis for the landslide detection. The NDVI represents the surface reflectance, which provides an estimate of the vegetation growth or loss, which may affect landslide occurrence. The PlanetScope

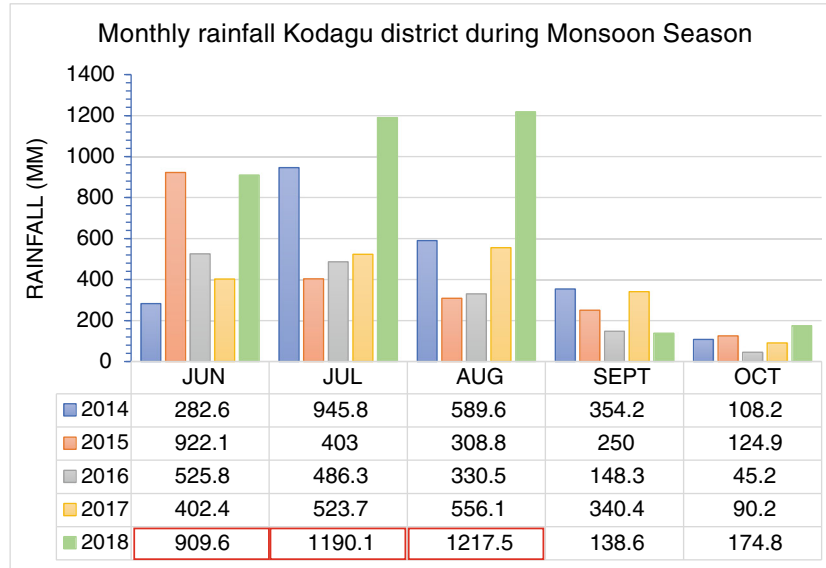


Fig. 2 Monthly rainfall (June–October) for the Kodagu districts in the Western Ghats of India (source: India Meteorological Department, Customized Rainfall Information System (CRIS)). The three red polygons show excess rainfall in the months of June, July, and August 2018

spectral bands were used to calculate the NDVI as the basis for the landslide modelling.

Slope

The selection of landslide-affecting factors depends on the local terrain conditions. We extracted the slope data from the 12.5-m resolution digital elevation model (DEM) that was created from the ALOS PALSAR data. The slope angle is crucial because the movement of mass is directly linked to the steepness of the slope, whereby steeper slopes are more prone to landslides. On the other hand, low angle slopes are more prone to the effects of channelized deposits, which results in rock fall and debris slides (Fan et al. 2018).

Convolution neural network

CNNs represent the state-of-the-art method in computer vision and image processing. Recently, CNNs have been applied in the domain of object detection and semantic segmentation due to the availability of labelled targeted images (Zhang et al. 2018). The use of CNNs is favourable for object detection and semantic segmentation because they have access to a large number of labelled images for training purposes, state-of-the-art algorithms, optimized CNN architectures, and GPUs (Guirado et al. 2017). Useful feature representations can be obtained by a CNN's multi-layer feed-forward neural networks, which allows the neural networks to recognize the feature differences in the image without using expert knowledge and defining rules (Ding et al. 2016). CNNs have a specific architecture, in which layers contain the pooling and convolutional layers, whereby the convolutional layers are considered to be the central part of a CNN architecture. The input image should be divided to the fixed window size patches for training the CNNs. The location of the centroid pixel of the window is selected based on the landslide bodies. Therefore, the fixed window size should be the minimum bounding box to cover the landslide in the

image patches. These image patches are convolved by several trainable kernels and produce feature maps. Pooling layers are frequently used after the convolutional layers to subsample the resulting feature maps. Although there are various types of pooling strategies, the max pooling is the most widely used pooling method. Using max pooling, the CNN model can keep the maximum values from the results of each convolution layer.

The primary operations performed in any CNN can be summarized by the following equation (Zhang et al. 2018):

$$O^l = P \left(\sigma(O^{l-1} * W^l + b^l) \right)$$

where P refers to the pooling layer and the O^{l-1} is the result of the convolution layers of the l th layer, W^l and the b^l represent the weights and biases of the layer, respectively, and $\sigma()$ indicates the non-linearity function outside the convolutional layer.

In this study, an input window size of 32×32 pixels was used for landslide detection. According to our landslide inventory, we had several small landslides with different shapes. Some are elongated and thin and can almost look like an unpaved road rather than a landslide. Most landslides exhibit a mixture of topographic features, which makes them difficult to recognize. This input window size was selected as the optimum size based on a cross-validation for our case study area. To account for variability in the topographic factors and optical data, we structured a CNN model and a kernel size that varies from 5×5 to 3×3 for convolutional layers using max pooling layers with a 2×2 kernel size (Fig. 4). Our structured CNN model was prepared and trained in Trimble's eCognition software (eCognition Developer 2020). The statistical gradient descent function was used to optimize weightings through the network. Experimental results showed that using a batch size of 50 along with a learning rate of 0.0001, 3000 epochs resulted in the best detection results.

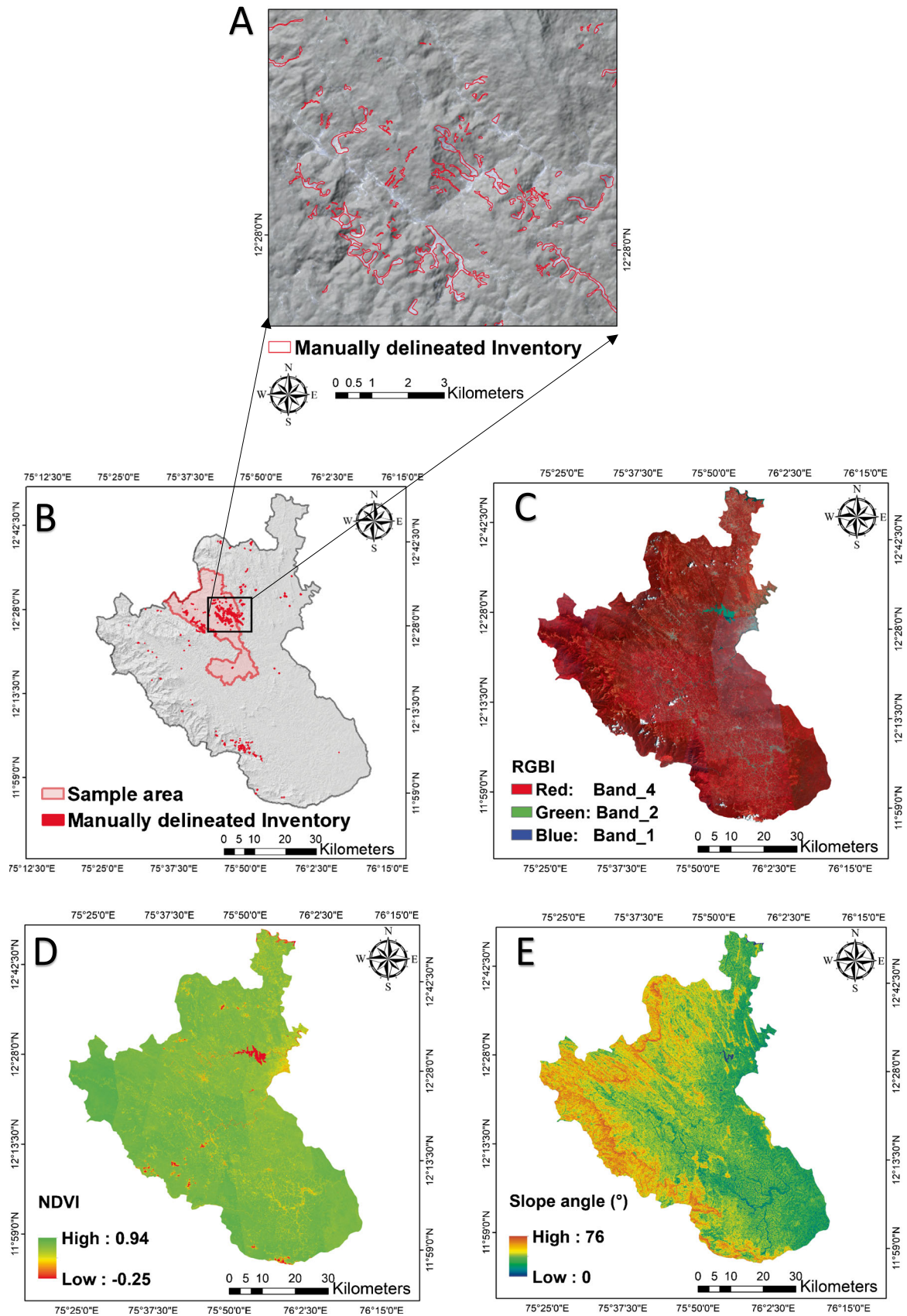


Fig. 3 (A) and (B) manually delineated landslide inventory prepared using visual image interpretation (C) false colour composite PlanetScope image, (D) normalized difference vegetation index (NDVI), and (E) slope angle

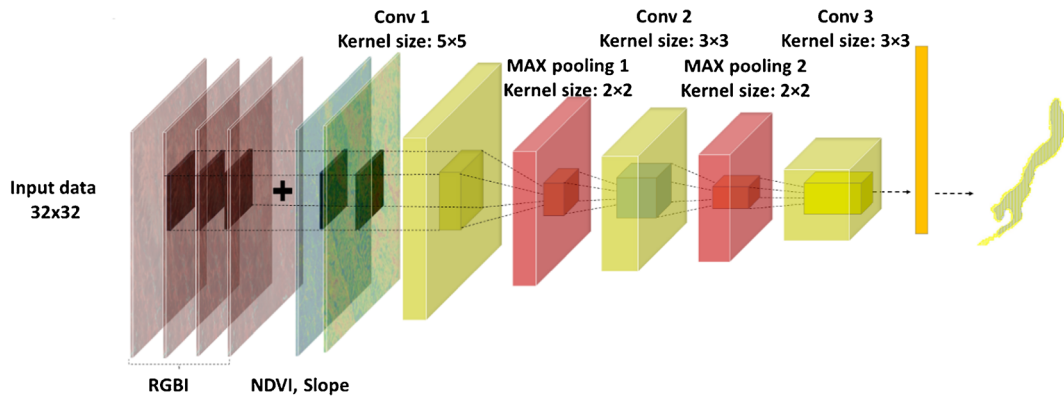


Fig. 4 The architecture of the CNN model, which is trained separately with two different training datasets

K-fold cross-validation

In this study, cross-validation was applied to determine the best model for landslide mapping and to decrease the negative effects of random sampling on the performances of the models. A fourfold cross-validation (CV) was applied based on various parameters such as the size of the database, different conditioning factors, and the number of computations within membership functions. The landslide-affected area was randomly divided into four equal folds of F1, F2, F3, and F4 where for any n and $m \in t$, size $F_n = \text{size } F_m$. The model runs k times and for any time of t , $t \leq k$. When the model runs at time t , 75% of the data without a subset of F_t was used for training the model, and 25% of the data was prepared for testing the model (Ghorbanzadeh et al. 2018). This method has been used by many researchers with various folds for different study goals. For example, Wiens et al. (2008) used a fivefold CV, and Ghorbanzadeh et al. (2019c) selected a fourfold CV for spatial prediction of wildfire susceptibility mapping. The distribution of our landslide inventory data within different four folds is shown in Fig. 5.

Landslide detection using CNNs

The architecture of the CNN model (Fig. 4) was trained with training datasets from outside the study site. Afterwards, the trained model was tested in the study site. We used the first CNN layer with a kernel size of five and continued with two CNN layers with a kernel size of three, adopted from Ghorbanzadeh et al. (2019a). The pooling layer was used to down sample the output of the CNN layer to produce a set of feature maps (Ghorbanzadeh et al. 2019a). The pooling layer reduces the spatial size of feature maps, thus reducing the computation volume for the remaining layers. In the CNN model, two max pooling layers of 2×2 were used. We fed our CNN model initially with a five-layer training dataset, including the optical data of the spectral bands RGBI and NDVI ($\text{CNN}_{\text{RGBI}, \text{N}}$), and then we added the topographic factor layer (slope steepness) to the previous dataset to train our $\text{CNN}_{\text{RGBI}, \text{N}, \text{S}}$ model. In the $\text{CNN}_{\text{RGBI}, \text{N}, \text{S}}$ model, we considered spectral bands along with the topographic factor (Fig. 6).

Comparison of landslide mapping using CNNs and manual detection

The trained CNN model was evaluated by employing to a sample area in Kodagu district. We used manually delineated

landslide boundaries as ground truth, which were prepared using visual image interpretation of pre- and post-event PlanetScope imagery and landslide point data provided by the Geological Survey of India. We compared the manually delineated landslide boundaries with the landslide inventory data generated by training the CNN model separately, once with five layers with optical data and then with six layers with optical data and the slope layer.

The visually interpreted landslide dataset was separated into training and validation datasets because using training data enables the model to provide better predictions, and validation of the landslides improves the accuracy of the model. Choosing the right data split is important for the best results. Therefore, in the landslide dataset, a random 75/25 ratio was chosen for training/validation data. Increasing the proportion of validation data would mean a decrease in the model's prediction accuracy, therefore, a 4-fold cross-validation process is considered optimal. It consists of a random split of the dataset into four folds. Three out of the four folds are chosen to perform model training, while the last quarter is used for validation. The process is repeated by choosing another set of quarters for validation and the three others for training. This process is repeated three times until all four groups have been used for validation (Fig. 5). The four accuracy assessments obtained are averaged into one overall accuracy assessment. Validation is performed with the whole dataset, but a given sample is never used for training and validation at the same time. At each stage of the 4-fold process, 75% of the dataset is randomly selected as training data, while the rest is left for validation.

A number of accuracy assessment approaches were used to assess the performance of the applied CNN model by evaluating the consistency between the CNN and manually mapped landslide inventory (Ghorbanzadeh et al. 2019b). In this study, the performance of the CNN model was ascertained using four different metrics (precision, recall, F1 score, and the Matthews correlation coefficient (MCC)), which are based on confusion matrices with true positives (TP), false positives (FP), and false negatives (FN) (Figs. 7 and 8).

The precision is the proportion of CNN-derived landslide pixels correctly identified as landslides (Lormand et al. 2018). The recall is the proportion of visually mapped landslide pixels

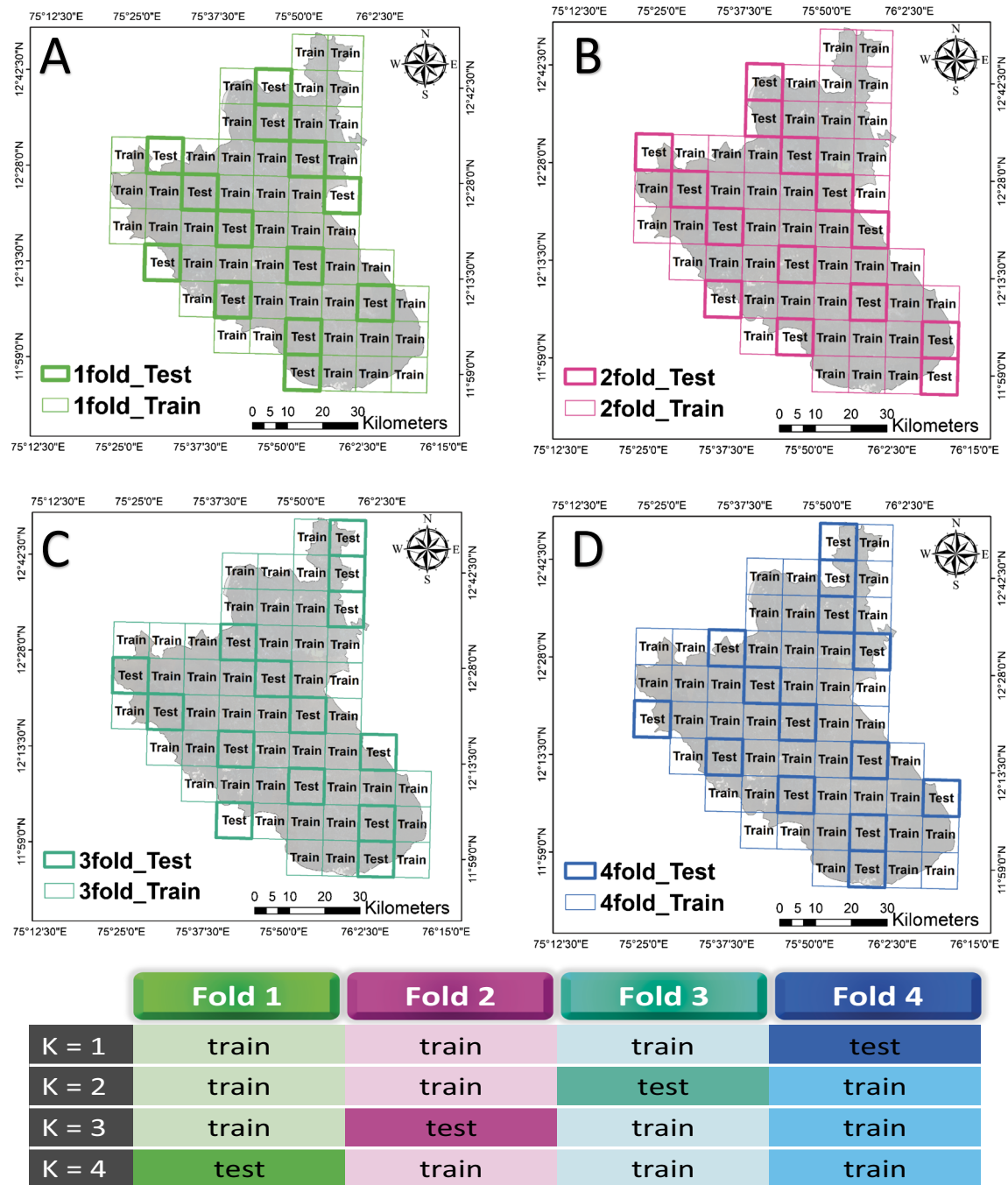


Fig. 5 (A, B, C, D) The applied fourfold cross-validation (CV) for the inventory dataset. Each colour represents a specific fold of the inventory dataset of the image patches both in the maps and in the table. The patches with bold text were used for testing, and the others were used for training the model

that were correctly detected by the CNNs (Liu et al. 2020). The F1 score is defined as the weighted harmonic mean of the precision and recall, used to evaluate the performance of the model (Liu et al. 2020). The higher the value of the F1 score, the better the performance of the model (Sameen and Pradhan 2019). The Matthews correlation coefficient (MCC) is useful to compare the binary classification of imbalanced datasets, and its values range from -1 to 1 , where 1 represents a perfect classifier and 0

represents a classifier with random detection (Prakash et al. 2020) (Tables 2 and 3).

Analysis of landslide mapping using frequency area distribution

Landslide inventories are statistically analysed using frequency area distribution (FAD) curves, in which landslide areas are plotted against the cumulative landslide frequencies. In a study by Malamud et al. (2004a), observations show that the power law

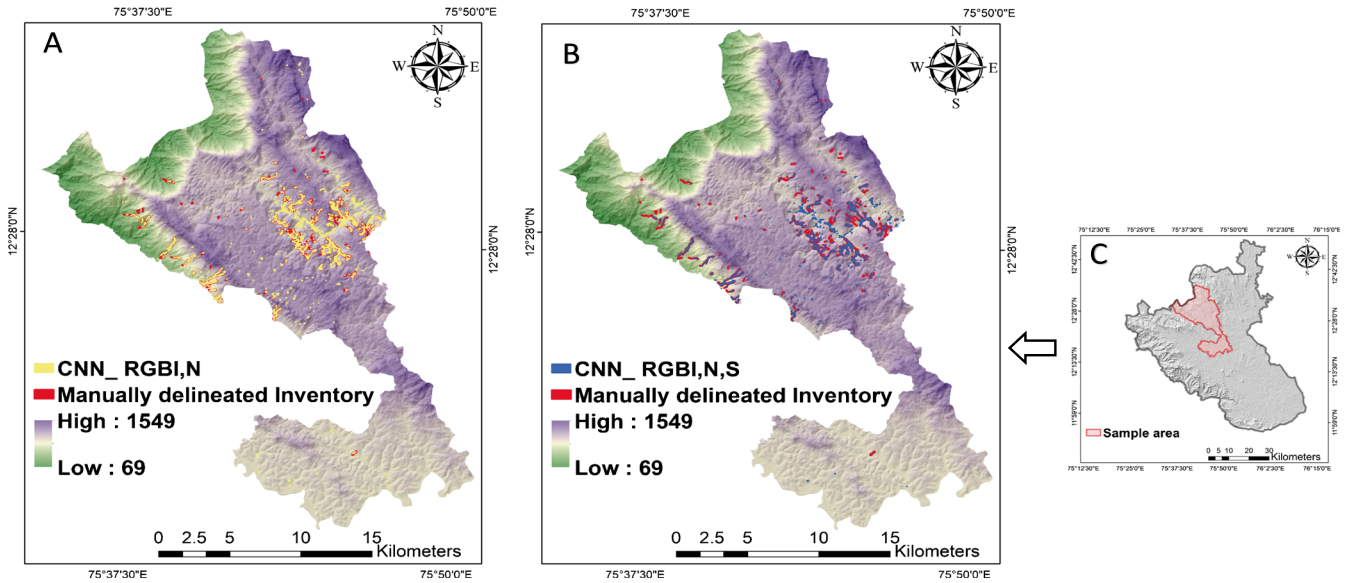


Fig. 6 Landslide detection results (A) CNN_RGBI, N and (B) CNN_RGBI, N, S; CNN_RGBI, N: convolutional neural network with RGB, infrared bands, and NDVI layer; CNN_RGBI, N, S: convolutional neural network with RGB, infrared bands, NDVI, and slope layer

applies for medium and large landslides. The probability of occurrence of a landslide of a particular size can be given by the power law equation:

$$p(x) = cX^{-\beta}$$

where X are observed values, c is a normalization constant, and β is the power law exponent.

Figure 9 shows the power law distribution for medium to large landslides and the divergence from the power law towards lower frequencies with a rollover point where the frequency decreases for smaller landslides. The trend of the FAD of most landslide inventories diverges from a power law for small landslides (Guzzetti et al. 2002; Malamud et al. 2004a; Stark and

Guzzetti 2009; Tanyaş et al. 2019). The point where this divergence begins is defined as the cut-off point (Stark and Hovius 2001; Tanyaş et al. 2019). According to Van Den Eeckhaut et al. (2007), in a power law distribution, the slope of the distribution is defined by a power law exponent. The part that is represented by large events is referred to as the power law tail, as shown in Fig. 9 (with a scaling parameter, β). Malamud et al. (2004a) investigated four well-documented landslide events and concluded that rollover is a real phenomenon in landslide inventories that depends upon the bias and under-sampling of the smaller landslides.

They modelled the FAD for these four inventories and established theoretical curves to estimate the total landslide area triggered by an earthquake or rainfall event.

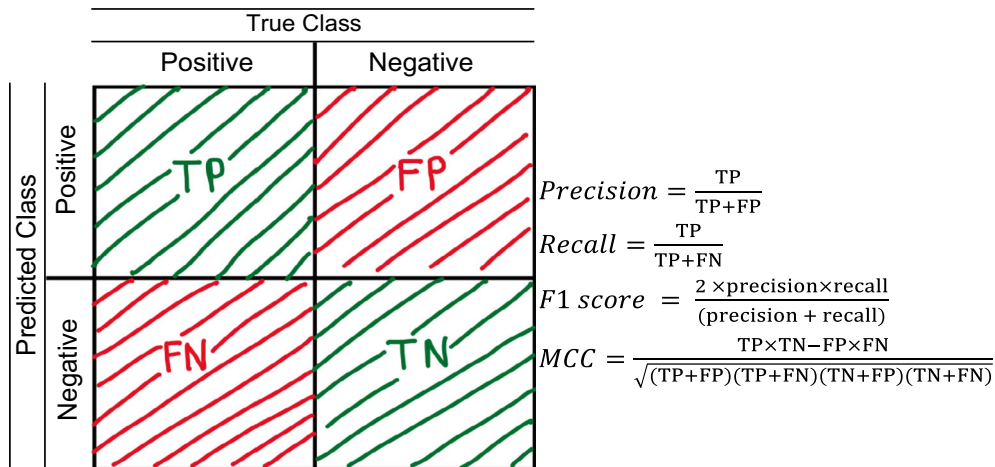


Fig. 7 Confusion matrix showing true class and predicted classes of landslides and other features and the four different metrics

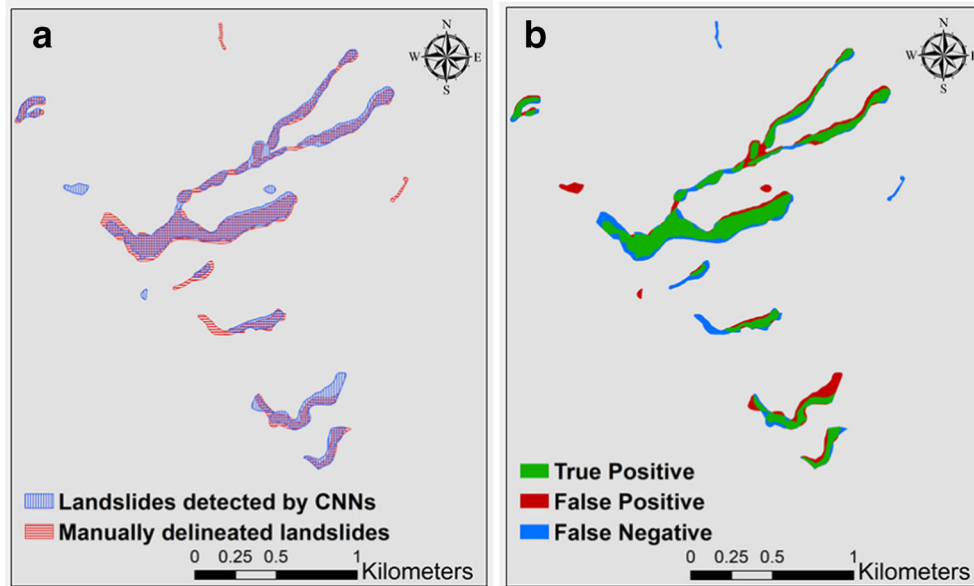


Fig. 8 (a) Inventory of landslide areas obtained from CNNs and manual delineation (b) true positive (TP), false positive (FP), and false-negative (FN) areas identified by comparing spatial overlaps between polygons of (a)

Malamud et al. (2004b) showed that the entire FAD of landslides could be explained by a three-parameter inverse gamma distribution (equation). This approach also described a way to estimate the landslide event magnitude (mLS). The mLS is the indication of the size of the landslide triggering event and gives an indication of the severity of the event in terms of landslide occurrence in a particular area for an event:

$$p(A_L; \rho, a, s) = \frac{1}{a\Gamma(\rho)} \left[\frac{a}{A_L - s} \right]^{\rho+1} \exp \left[-\frac{a}{A_L - s} \right]$$

where ρ is the parameter primarily controlling power law decay for medium and large values, $\Gamma(\rho)$ is the gamma function of ρ , A_L is landslide area, a is the location of rollover point, s is the exponential decay for small landslide areas, and $-(\rho + 1)$ is the power law exponent. Malamud et al. (2004b) provided a best fit for the power law exponent and showed that $-(\rho + 1) = 2.4$.

Table 4 shows that the power law exponent of the analysed folds for CNN-derived inventories ranges from 1.37 to 2.22, which is

lower than 'the given power law function exponent of 2.4' reported by Malamud et al. (2004b). Lower power law exponent values are lower as a result of using smaller dataset for analysis, as Malamud et al. (2004b) used three large landslide inventories from around the world. The smallest landslide areas mapped ranged from 2491 to 9407 m², and the largest landslides mapped range from 47,695.36 to 528,042.68 m² for the CNN-derived landslide inventories (see Table 4).

There is a scattered pattern of the plotted landslide probability density to the inverse gamma fit (see Fig. 10). Differences in the probability distribution and inverse gamma fit could result from gaps in the data of mapped landslides for given inventories, which means that some smaller landslides are missing or not mapped by the CNN model. The rollover points differ between inventories. For manual and CNN-derived inventories, the rollover points for smaller landslides vary between 454.84 and 10,125.55 m². In the CNN model-derived inventories, the rollover point ranges between 10,125.55 and 17,345.80 m², which is larger than manually delineated landslides because our model was not able to detect smaller landslides efficiently because of constraints in training

Table 2 The results of landslide detection in the study area based on the CNN model trained CNN_RGBI, N: convolutional neural network with RGB, infrared bands, and NDVI layer

Fold	TP (ha)	FP (ha)	FN (ha)	Precision (%)	Recall (%)	F1measure (%)	MCC (%)
1-fold	15.70	9.18	7.79	63.1	66.8	64.9	64.9
2-fold	135.10	70.87	88.00	65.6	60.6	63.0	62.9
3-fold	139.30	64.02	59.47	68.5	70.1	69.3	69.2
4-fold	72.24	41.15	42.16	63.7	63.1	63.4	63.4
Mean				65.2	65.1	65.1	65.1

Accuracies are stated as precision, recall, F1-measure, and MCC

Table 3 The results of landslide detection in the study area based on the CNN model trained CNN_RBGI, N, S: convolutional neural network with RGB, infrared bands, NDVI, and slope layers

Fold	TP (ha)	FP (ha)	FN (ha)	Precision (%)	Recall (%)	F1measure (%)	MCC (%)
1-fold	14.65	16.83	3.83	46.5	79.3	58.6	60.7
2-fold	150.26	95.18	62.39	63.8	73.8	68.4	68.5
3-fold	150.11	73.97	41.50	70.6	79.6	74.9	75.0
4-fold	86.88	54.15	24.81	63.8	78.6	70.4	70.8
Mean				61	78	68	68.8

Accuracies are stated as precision, recall, F1-score, and MCC

samples due to the smaller size of the study area. For smaller landslides, fold 2 shows more effectiveness, and for larger landslides, fold 3 shows more effectiveness as can be seen in power law tail in Fig. 10.

Discussion

This paper presents an approach to mapping landslides using a CNN in the hilly terrain regions of the Western Ghats in India. We used a simple CNN architecture with five and six input layers to train the model. We designed the CNN architecture using minimal input data for landslide detection in the study area. In recent studies, CNNs outperformed traditional machine learning algorithms in the detection of landslides (Liu et al. 2020; Ye et al. 2019). However, designing a CNN architecture and optimizing its parameters using sample strategies remain

challenging tasks (Ghorbanzadeh et al. 2019a). We only used slope data as auxiliary topographical input information to remove the errors caused by spectral similarities in riverbeds and the built-up area in moderate slopes. The CNN model was trained with data, including the slope layer, which performed better than when using optical data alone by about 2.9 F1 score and 3.7 MCC mean values (Mondini et al. 2013). This higher accuracy is due to fewer FPs (almost half), which is attributed to the fact that the CNN model was trained with the slope data. The resulting accuracies of our designed CNN architecture are comparable with published studies that were based on much more complex CNN architectures, such as the U-Net and residual networks (Prakash et al. 2020).

The accuracy assessment metrics used for the validation of the landslide detection in this study demonstrate that using the CNN

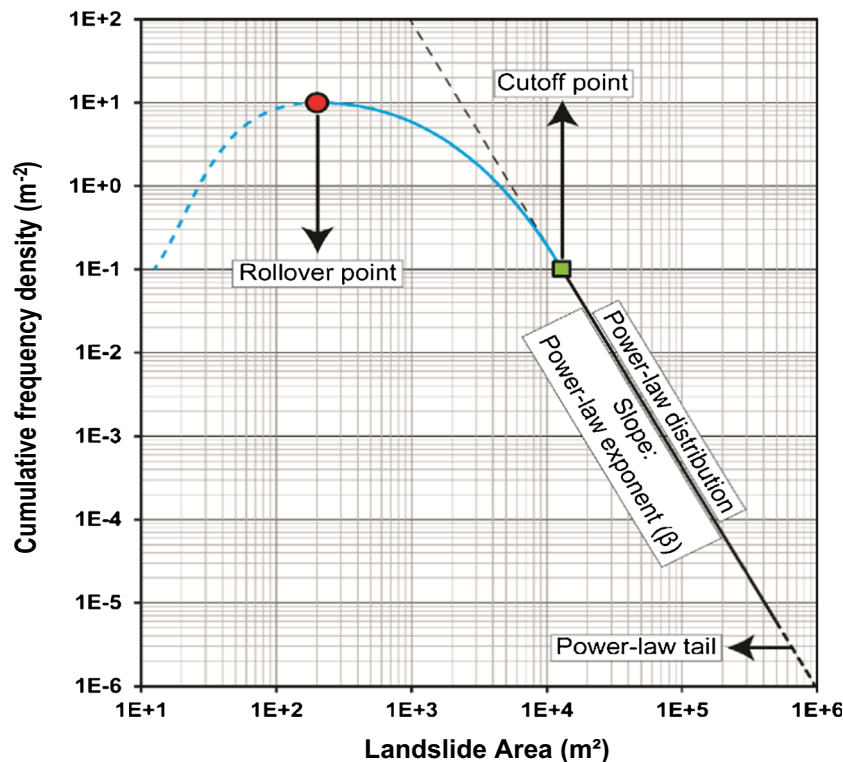


Fig. 9 Schematic representation of the main components of a cumulative frequency area distribution for (FAD) for a landslide inventory (Malamud et al. 2004a)

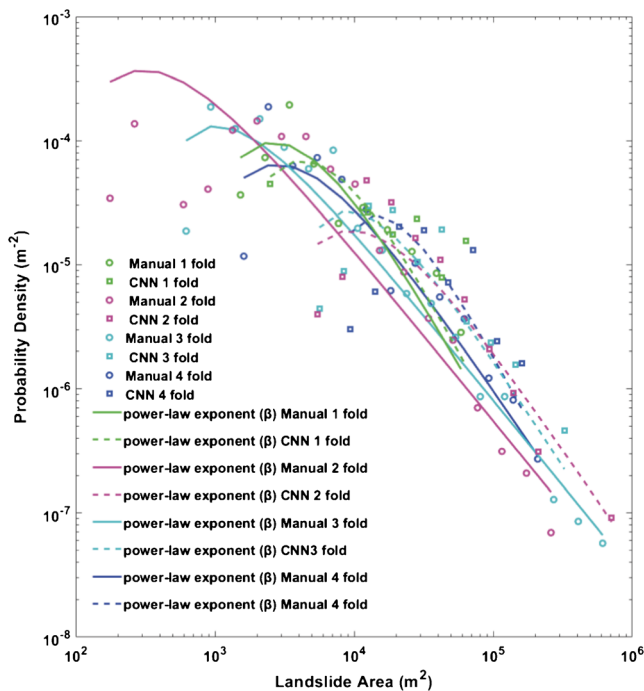
Table 4 Comparison of the frequency area statistics of landslide area

Inventories	Total number of landslides N_{LT}	Total area of landslides A_L km ²	Minimum area of landslides min A_L m ²	Maximum area of landslides max A_L m ²	Power law exponent (β)	Rollover point (m ²)
Manual 1-fold	18	0.23	1524	39,370.03	2.02	5744.82
Manual 2-fold	167	2.03	176	446,831.61	1.37	454.84
Manual 3-fold	86	4.02	621	203,949.08	1.38	1287.01
Manual 4-fold	53	1.13	1610	146,899.24	1.66	5107.21
CNN 1-fold	9	0.24	2491	47,695.36	2.22	10,125.55
CNN 2-fold	46	2.05	5469	528,042.68	1.66	17,345.80
CNN 3-fold	40	1.90	5629	234,587.59	1.75	14,021.63
CNN 4-fold	35	1.04	9407	141,198.62	2.21	27,447

model provides automatic rainfall-induced landslide detection and inventory mapping using remote sensing data. However, it is not appropriate comparing our results with those from other studies in the Western Ghats, which used other object-based models for landslide detection and modelling (Martha et al. 2019). In this study, our model was trained with optical data from PlanetScope imagery with 3-m spatial resolution, whereas Martha et al. (2019) used Resourcesat-2,2A LISS-IV multispectral data with 5.8-m spatial resolution. The use of different datasets

seems to produce differences in the detected landslides, especially because only the unvegetated areas were mapped and the connections were often not detected because of shadows and vegetation (Fiorucci et al. 2019). The model training strategy differs between CNN and other machine learning and object-based models. Adding additional heterogeneous training data usually reduces the convergence capabilities of a CNN model and, consequently, causes generalization and reduces the overall accuracy. However, by adding the slope data for training, the applied CNN model was able to decrease the false positives by distinguishing the landslide areas from non-vegetated areas such as the riverbeds, bare land, and built-up areas (Fig. 11). In our study, a total of 343 landslides were mapped as polygons, covering an area of 4140 km². The landslides along the riverbeds were difficult to detect using our CNN architecture. Also, water body and settlements areas were considered false positives in the model. There are some errors in the CNN slide detection results in built-up areas, forests, along the road network, and in riverbeds. A total of 14 polygons were false positives, whereby 6 were in forests, 6 in riverbeds, and one false positive each in built-up areas and along the road network. The false positives in forests cover an area of 11,937.6 m², which is about 2.04% of the CNN result. Similarly, the false positives in the built-up areas and road networks make up about 0.19% and 0.22% of the area of the CNN results, respectively. Most false positives were in riverbeds, which make up about 4.5% (2,656,085 m²) of the CNN result. False positives in our results could be due to having fewer training samples in those classes because the size of our study area is smaller.

The vegetation plays a huge role in detection of landslides as the model can distinguish the boundaries of landslides apart from vegetated areas using NDVI layer. Another limitation of our model was that it merged several individual landslides into one landslide. The fact that a number of landslides were mapped is attributed to the amalgamation of landslides due to merging of debris flows and slides after the event. The amalgamation of landslides is an issue that can be overcome in future studies with novel and optimized CNN architectures.

**Fig. 10** Landslide frequency size distribution, representing the dependence of landslide probability density on the landslide area

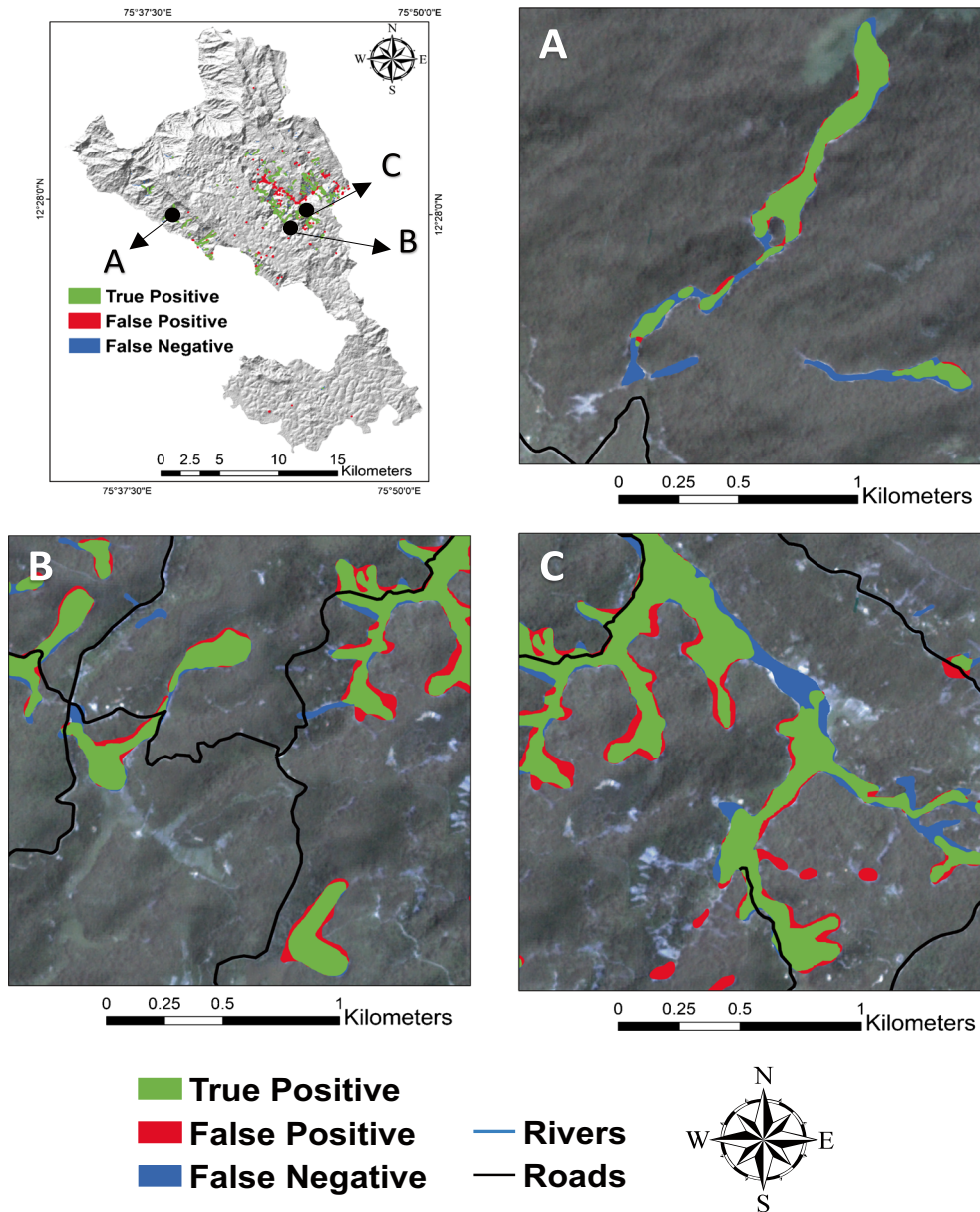


Fig. 11 Enlarged maps of the results of the CNN model, showing the detection of true and false positives and false negatives in the testing area: (A) forest area, (B) near-road network and hilly terrain area, and (C) near built-up areas

Conclusions

The main contribution of the present study is the automatic detection of landslides after major triggering events such as monsoon rainfalls. However, the main limitation for such study areas is having access to cloud-free images during the rainfall season. Developing semi- or fully automated approaches for landslide mapping is needed due to the substantially increasing frequency of natural disasters in recent years, causing significant concerns about the loss of human lives. In the selected study area, the loss of properties was mainly due to rainfall-induced landslides.

The occurrences of landslides worldwide are expected to increase due to urbanization, deforestation, and continued anthropogenic activities. Climate change has also contributed to variations or fluctuations in precipitation in the landslide-prone

areas. Our study represents the semi-automatic rainfall-induced landslide detection and inventory mapping using remote sensing data for Kodagu district, which lies in the Western Ghats of India. We developed a CNN model to detect landslides based on various input data, including spectral information and the topographical slope factor. Our applied CNN model structure is simple and may not be superior to those used in previous studies listed in Table 1. However, our approach requires less human participation and can thus be considered a semi-automatic approach. The applied methodology is easily transferable to similar regions, like the Himalayas, and our trained model can also be used for a new landslide inventory dataset. However, in regions with less vegetation cover or steeper terrain, the model might require retraining based on the landslide inventory from these areas, which will

enhance the performance of the model. Moreover, the methodology can be used for detecting landslides caused by other triggering processes, e.g., earthquake-induced landslides. Therefore, this study and the applied methodology are useful for landslide inventory mapping and, consequently, for disaster mitigation management.

Acknowledgements

The authors are also grateful to the anonymous reviewers and the editor for their valuable comments/suggestions which have helped us to improve an earlier version of the manuscript.

Funding

Open Access funding provided by Paris Lodron University of Salzburg. This research was partly funded by the Austrian Science Fund (FWF) through the Doctoral College GIScience (DK W1237-N23) at the University of Salzburg—Open Access Funding by the Austrian Science Fund (FWF).

Open Access This article is licensed under a Creative Commons Attribution 4.0 International License, which permits use, sharing, adaptation, distribution and reproduction in any medium or format, as long as you give appropriate credit to the original author(s) and the source, provide a link to the Creative Commons licence, and indicate if changes were made. The images or other third party material in this article are included in the article's Creative Commons licence, unless indicated otherwise in a credit line to the material. If material is not included in the article's Creative Commons licence and your intended use is not permitted by statutory regulation or exceeds the permitted use, you will need to obtain permission directly from the copyright holder. To view a copy of this licence, visit <http://creativecommons.org/licenses/by/4.0/>.

References

Chen Z, Zhang Y, Ouyang C, Zhang F, Ma J (2018) Automated landslides detection for mountain cities using multi-temporal remote sensing imagery *Sensors* 18:821

Cruden DM, Varnes DJ (1996) Landslides: investigation and mitigation

Das I, Stein A, Kerle N, Dadhwal VK (2011) Probabilistic landslide hazard assessment using homogeneous susceptible units (HSU) along a national highway corridor in the northern Himalayas. *India Landslides* 8:293–308. <https://doi.org/10.1007/s10346-011-0257-9>

Ding A, Zhang Q, Zhou X, Dai B (2016) Automatic recognition of landslide based on CNN and texture change detection. In: 2016 31st Youth Academic Annual Conference of Chinese Association of Automation (YAC), IEEE, pp 444–448

Du Z, Yang J, Ou C, Zhang T (2019) Smallholder crop area mapped with a semantic segmentation deep learning method *Remote Sensing* 11:888

Duro DC, Franklin SE, Dubé MG (2012) A comparison of pixel-based and object-based image analysis with selected machine learning algorithms for the classification of agricultural landscapes using SPOT-5 HRG imagery. *Remote Sens Environ* 118:259–272. <https://doi.org/10.1016/j.rse.2011.11.020>

eCognition Developer T (2020) “eCognition Developer User Guide”

Eskandari S, Reza Jaafari M, Oliva P, Ghorbanzadeh O, Blaschke T (2020) Mapping land cover and tree canopy cover in Zagros forests of Iran: application of Sentinel-2, Google Earth, and Field Data *Remote Sensing* 12:1912

Fan X, Domènech G, Scaringi G, Huang R, Xu Q, Hales TC, Dai L, Yang Q, Francis O (2018) Spatio-temporal evolution of mass wasting after the 2008 Mw 7.9 Wenchuan earthquake revealed by a detailed multi-temporal inventory. *Landslides* 15:2325–2341

Fayne JV, Ahamed A, Roberts-Pierel J, Rumsey AC, Kirschbaum DJEI (2019) Automated satellite-based landslide identification product for Nepal 23:1–21

Fiorucci F, Ardizzone F, Mondini AC, Viero A, Guzzetti F (2019) Visual interpretation of stereoscopic NDVI satellite images to map rainfall-induced landslides. *Landslides* 16:165–174. <https://doi.org/10.1007/s10346-018-1069-y>

Ghorbanzadeh O, Blaschke T, Gholamnia K, Meena SR, Tiede D, Aryal J (2019a) Evaluation of different machine learning methods and deep-learning convolutional neural networks for landslide detection *Remote Sensing* 11:196

Ghorbanzadeh O, Meena SR, Blaschke T, Aryal J (2019b) UAV-based slope failure detection using deep-learning convolutional neural networks *Remote Sensing* 11:2046

Ghorbanzadeh O, Rostamzadeh H, Blaschke T, Gholamnia K, Aryal J (2018) A new GIS-based data mining technique using an adaptive neuro-fuzzy inference system (ANFIS) and k-fold cross-validation approach for land subsidence susceptibility mapping. *Nat Hazards* 94:497–517. <https://doi.org/10.1007/s11069-018-3449-y>

Ghorbanzadeh O, Valizadeh Kamran K, Blaschke T, Aryal J, Naboureh A, Einali J, Bian J (2019c) Spatial prediction of wildfire susceptibility using field survey GPS data and machine learning approaches 2:43

Guirado E, Tabik S, Alcaraz-Segura D, Cabello J, Herrera F (2017) Deep-learning convolutional neural networks for scattered shrub detection with Google Earth imagery *arXiv preprint arXiv:1706.00917*

Guzzetti F, Carrara A, Cardinali M, Reichenbach P (1999) Landslide hazard evaluation: a review of current techniques and their application in a multi-scale study. *Central Italy Geomorphology* 31:181–216. [https://doi.org/10.1016/S0169-555X\(99\)00078-1](https://doi.org/10.1016/S0169-555X(99)00078-1)

Guzzetti F, Malamud BD, Turcotte DL, Reichenbach P (2002) Power-law correlations of landslide areas in central Italy. *Earth Planet Sci Lett* 195:169–183. [https://doi.org/10.1016/S0012-821X\(01\)00589-1](https://doi.org/10.1016/S0012-821X(01)00589-1)

Guzzetti F, Mondini AC, Cardinali M, Fiorucci F, Santangelo M, Chang K-T (2012) Landslide inventory maps: new tools for an old problem. *Earth Sci Rev* 112:42–66. <https://doi.org/10.1016/j.earscirev.2012.02.001>

Jin B, Ye P, Zhang X, Song W, Li S (2019) Object-oriented method combined with deep convolutional neural networks for land-use-type classification of remote sensing images. *J Indian Soc Remote Sensing* 47:951–965. <https://doi.org/10.1007/s12524-019-00945-3>

Juang CS, Stanley TA, Kirschbaum DB (2019) Using citizen science to expand the global map of landslides: introducing the cooperative open online landslide repository (COOLR). *PLoS One* 14:e0218657

Lei T, Zhang Y, Lv Z, Li S, Liu S, Nandi AK (2019) Landslide inventory mapping from bitemporal images using deep convolutional neural networks *IEEE Geoscience and Remote Sensing Letters* 16:982–986. doi:<https://doi.org/10.1109/LGRS.2018.2889307>

Liu P, Wei Y, Wang Q, Chen Y, Xie J (2020) Research on post-earthquake landslide extraction algorithm based on improved U-Net model. *Remote Sens* 12:894

Liu S, Qi Z, Li X, Yeh AG-O (2019) Integration of convolutional neural networks and object-based post-classification refinement for land use and land cover mapping with optical and SAR data. *Remote Sens* 11:690

Lormand C, Zellmer GF, Németh K, Kilgour G, Mead S, Palmer AS, Sakamoto N, Yurimoto H, Moebis A (2018) Weka trainable segmentation plugin in ImageJ: a semi-automatic tool applied to crystal size distributions of microlites in volcanic rocks. *Microsc Microanal* 24:667–675. <https://doi.org/10.1017/S1431927618015428>

Lu P, Stumpf A, Kerle N, Casagli N (2011) Object-oriented change detection for landslide rapid mapping. *IEEE Geosci Remote Sens Lett* 8:701–705. <https://doi.org/10.1109/LGRS.2010.2101045>

Malamud BD, Turcotte DL, Guzzetti F, Reichenbach P (2004a) Landslide inventories and their statistical properties. *Earth Surf Process Landf* 29:687–711

Malamud BD, Turcotte DL, Guzzetti F, Reichenbach P (2004b) Landslides, earthquakes, and erosion. *Earth Planet Sci Lett* 229:45–59

Martha TR, Kerle N, Jetten V, van Westen CJ, Kumar KV (2010) Characterising spectral, spatial and morphometric properties of landslides for semi-automatic detection using object-oriented methods. *Geomorphology* 116:24–36. <https://doi.org/10.1016/j.geomorph.2009.10.004>

Martha TR, Roy P, Khanna K, Mrinalni K, Kumar KV (2019) Landslides mapped using satellite data in the Western Ghats of India after excess rainfall during August 2018. *Curr Sci* 117:804–812

Meena SR, Ghorbanzadeh O, Hölbling D (2019) Comparison of event-based landslide inventories: a case study from Gorkha earthquake 2015, Nepal. Paper presented at the European Space Agency's 2019 Living Planet Symposium, Milan, Italy,

Moine M, Puissant A, Malet J-P Detection of landslides from aerial and satellite images with a semi-automatic method. Application to the Barcelonnette basin (Alpes-de-Hautes-Provence, France). In: 2009

Mondini AC, Marchesini I, Rossi M, Chang K-T, Pasquariello G, Guzzetti F (2013) Bayesian framework for mapping and classifying shallow landslides exploiting remote sensing

- and topographic data. *Geomorphology* 201:135–147. <https://doi.org/10.1016/j.geomorph.2013.06.015>
- Pradhan B, Singh R, Buchroithner M (2006) Estimation of stress and its use in evaluation of landslide prone regions using remote sensing data *Advances in Space Research* 37:698–709
- Prakash N, Manconi A, Loew S (2020) Mapping landslides on EO data: performance of deep learning models vs. traditional machine learning models *Remote Sensing* 12:346
- Qayyum A, Malik A, Saad MN, Mazher M (2019) Designing deep CNN models based on sparse coding for aerial imagery: a deep-features reduction approach. *Eur J Remote Sen* 52:221–239
- Ramachandra T, Bharath S, Vinay SJPiDS (2019) Visualisation of impacts due to the proposed developmental projects in the ecologically fragile regions-Kodagu district, Karnataka 3:100038
- Sameen MI, Pradhan B (2019) Landslide detection using residual networks and the fusion of spectral and topographic information. *IEEE Access* 7:114363–114373
- Shahabi H, Jarihani B, Tavakkoli Piralilou S, Chittleborough D, Avand M, Ghorbanzadeh O (2019) A semi-automated object-based gully networks detection using different machine learning models: a case study of Bowen catchment, Queensland, Australia *Sensors* 19:4893
- Stark CP, Guzzetti F (2009) Landslide rupture and the probability distribution of mobilized debris volumes. *J Geophys Res Earth Surf* 114:1–16. <https://doi.org/10.1029/2008JF001008>
- Stark CP, Hovius N (2001) The characterization of landslide size distributions. *Geophys Res Lett* 28:1091–1094. <https://doi.org/10.1029/2000GL008527>
- Tanyaş H, van Westen CJ, Allstadt KE, Jibson RW (2019) Factors controlling landslide frequency–area distributions. *Earth Surf Process Landf* 44:900–917. <https://doi.org/10.1002/esp.4543>
- Tavakkoli Piralilou S et al. (2019) Landslide detection using multi-scale image segmentation and different machine learning models in the higher Himalayas *Remote Sensing* 11:2575
- Van Den Eeckhaut M, Poesen J, Govers G, Verstraeten G, Demoulin A (2007) Characteristics of the size distribution of recent and historical landslides in a populated hilly region. *Earth Planet Sci Lett* 256:588–603. <https://doi.org/10.1016/j.epsl.2007.01.040>
- Vinutha D (2015) Geomorphology and natural hazards in parts of Coorg district Karnataka state
- Wiens TS, Dale BC, Boyce MS, Kershaw GP (2008) Three way k-fold cross-validation of resource selection functions *Ecological Modelling* 212:244–255. <https://doi.org/10.1016/j.ecolmodel.2007.10.005>
- Xu C, Tian Y, Zhou B, Ran H, Lyu G (2017) Landslide damage along Araniko highway and Pasang Lhamu highway and regional assessment of landslide hazard related to the Gorkha, Nepal earthquake of 25 April 2015. *Geoenvironmental Disasters* 4:14–14. <https://doi.org/10.1186/s40677-017-0078-9>
- Ye C et al. (2019) Landslide detection of hyperspectral remote sensing data based on deep learning with constraints. *IEEE Journal of Selected Topics in Applied Earth Observations and Remote Sensing*:1–14. doi:<https://doi.org/10.1109/JSTARS.2019.2951725>
- Zhang C, Sargent I, Pan X, Li H, Gardiner A, Hare J, Atkinson PM (2018) An object-based convolutional neural network (OCNN) for urban land use classification. *Remote Sens Environ* 216:57–70. <https://doi.org/10.1016/j.rse.2018.06.034>

S. R. Meena · O. Ghorbanzadeh · T. G. Nachappa · T. Blaschke

Department of Geoinformatics—Z_GIS,
University of Salzburg,
5020, Salzburg, Austria
Email: sansarraj.meena@sbg.ac.at

S. R. Meena · C. J. van Westen

Faculty of Geoinformation Science and Earth Observation (ITC),
University of Twente,
Enschede, The Netherlands

R. P. Singh

School of Life and Environmental Sciences, Schmid College of Science and Technology,
Chapman University One University Drive,
Orange, CA, USA

R. Sarkar

Department of Civil Engineering,
Delhi Technological University,
Bawana Road, Delhi, India